Muscle Synergies Modify Optimization Estimates of Joint Stiffness During Walking

Mohammad S. Shourijeh
Department of Mechanical Engineering,
Rice University,
6100 Main Street,
Houston, TX 77005
e-mail: shourijeh@rice.edu

Benjamin J. Fregly
Mem. ASME
Department of Mechanical Engineering,
Rice University,
6100 Main Street,
Houston, TX 77005
e-mail: fregly@rice.edu

Because of its simplicity, static optimization (SO) is frequently used to resolve the muscle redundancy problem (i.e., more muscles than degrees-of-freedom (DOF) in the human musculoskeletal system). However, SO minimizes antagonistic co-activation and likely joint stiffness as well, which may not be physiologically realistic since the body modulates joint stiffness during movements such as walking. Knowledge of joint stiffness is limited due to the difficulty of measuring it experimentally, leading researchers to estimate it using computational models. This study explores how imposing a synergy structure on the muscle activations estimated by optimization (termed "synergy optimization," or SynO) affects calculated lower body joint stiffnesses during walking. By limiting the achievable muscle activations and coupling all time frames together, a synergy structure provides a potential mechanism for reducing indeterminacy and improving physiological co-activation but at the cost of a larger optimization problem. To compare joint stiffnesses produced by SynO (2–6 synergies) and SO, we used both approaches to estimate lower body muscle activations and forces for sample experimental overground walking data obtained from the first knee grand challenge competition. Both optimizations used a custom Hill-type muscle model that permitted analytic calculation of individual muscle contributions to the stiffness of spanned joints. Both approaches reproduced inverse dynamic joint moments well over the entire gait cycle, though SynO with only two synergies exhibited the largest errors. Maximum and mean joint stiffnesses for hip and knee flexion in particular decreased as the number of synergies increased from 2 to 6, with SO producing the lowest joint stiffness values. Our results suggest that SynO increases joint stiffness by increasing muscle co-activation, and furthermore, that walking with a reduced number of synergies may result in increased joint stiffness and perhaps stability.
[DOI: 10.1115/1.4044310]

Keywords: muscle synergies, motor modules, musculoskeletal modeling, static optimization, synergy optimization, muscle stiffness, joint stiffness

Introduction

Reliable estimation of muscle forces during human movement could facilitate the development of improved interventions for disorders such as osteoarthritis, stroke, cerebral palsy, and Parkinson's disease [1]. Since muscle forces cannot be measured noninvasively using standard experimental methods, numerous research studies have used computational models to estimate these quantities. However, the human musculoskeletal system is statically indeterminate, meaning more muscles are present than the number of degrees-of-freedom (DOF) in the skeleton (i.e., the muscle redundancy problem). For this reason, rigid body dynamics alone cannot be used to solve for unique muscle activations and forces, necessitating the development of more complex computational approaches.

Due to its simplicity, static optimization (SO) is the most commonly used computational approach for estimating unique muscle activations and forces during human movement. The two most common competing approaches are dynamic optimization and electromyogram (EMG)-driven modeling. Whereas dynamic optimization utilizes forward skeletal dynamics, solves for muscle activations over all time frames simultaneously, and can predict new motions [2–4], SO utilizes inverse skeletal dynamics, solves for muscle activations at each time frame independently, and requires measured motion and external forces as inputs. Though dynamic optimization possesses potential advantages over SO [4–6], for slow to moderate speed activities such as gait, estimated muscle activations and forces from the two approaches are practically equivalent [7,8]. EMG-driven modeling approaches have also been used to estimate muscle forces during human movement [9–13]. These approaches require experimental EMG data as inputs and calibrate muscle-tendon model parameters. However, due to uncertainties in measured EMG signals (e.g., cross talk [14,15], movement artifact [16], processing parameters [17], and normalization [18]), the accuracy of the estimated muscle forces remains unknown [19]. In contrast to EMG-driven modeling, SO does not require any EMG data as inputs and typically is not used to perform calibration of muscle model parameters.

The simplifications provided by SO come at the cost of less physiologically realistic solutions. The most commonly used SO cost function is minimization of the sum of squares of muscle activations [3,19–21], which is the default SO cost function in OPENSIM [22]. The resulting minimum effort solution produces minimum muscle co-activation between agonistic and antagonist muscles [23,24] and consequently minimum joint stiffness (i.e., resistance of a joint to move in response to an applied moment [25]). Since recent research has suggested that the central nervous system modulates joint stiffness during movement [26,27], and specifically during gait to control stability or absorb impacts [26], a minimum co-activation solution may be a poor representation of an individual's actual motor control strategy.

Recently, researchers have begun exploring muscle synergy concepts as a way to limit the achievable muscle activations predicted by optimization methods [28–39], thereby reducing solution indeterminacy and increasing physiological co-activation. Analysis of experimental EMG data provides a muscle synergy

[1]Corresponding author.
Manuscript received March 11, 2019; final manuscript received July 1, 2019; published online October 1, 2019. Assoc. Editor: Sara Wilson.

control structure [40–43], where muscle synergies can be viewed as a low-dimensional set of neural control building blocks that are used to construct a higher dimensional set of measured EMG signals. Each muscle synergy consists of a time-varying neural command and a time-invariant vector of weights that defines how the neural command contributes to each EMG signal. Typically between 2 and 6, muscle synergies are needed to account for over 90% of the variability in all measured EMG signals during human movement [32,35,44,45]. Though several studies have imposed a synergy structure on their muscle excitations or activations estimated by optimization methods [30,31,35–39], no study to date has investigated how imposing a synergy structure on estimated muscle controls affects calculated joint stiffnesses.

This study investigates how incorporating an explicit muscle synergy control structure into an optimization problem formulation affects calculated lower body joint stiffnesses, as well as net joint moment matching, muscle co-activation, and muscle force, during walking. To perform the investigation, similar to Ref. [36], we modified the common SO problem formulation that minimizes the sum of squares of muscle activations for each time frame independently into a formulation that minimizes the sum of squares of muscle activations plus the sum of squares of joint moment matching errors over all time frames simultaneously. Whereas SO uses muscle activations as design variables, our modified formulation (terms "synergy optimization," or SynO) uses synergy activations and their associated synergy vectors as design variables, where the time-invariant synergy vectors couple the time frames together. To estimate the resulting joint stiffnesses, we also developed an analytical joint stiffness formulation based on a rigid-tendon Hill-type muscle model. Joint stiffness along with joint moment matching, muscle activation, and muscle force results found using 2–6 synergies are compared with SO results to demonstrate the effects of a synergy control structure.

Methods

Musculoskeletal Model Creation. The experimental walking data used in this study were taken from the First Grand Challenge Competition to Predict in vivo Knee Loads [46]. The subject (coded JW, male, age 83, mass 68 kg, height 1.66 m) possessed a right total knee replacement and neutral leg alignment. One normal gait cycle (jw_ngait_2), defined from heel strike to subsequent heel strike of the right leg, was selected for analysis. Surface marker trajectory and ground reaction force data were taken from this trial.

A previously developed pelvis and right leg OPENSIM model of the subject [39] was used for analyses performed in OPENSIM [22]. Therefore, the left leg was not analyzed in this study. The model possessed three hip DOFs, one knee DOF, and two ankle DOFs and incorporated geometry constructed from the subject's CT scan data and CAD models of the subject's knee implant components. The origins, insertions, and wrapping surfaces of 44 muscle-tendon actuators were taken from a scaled generic OPENSIM model [47] and transferred to the subject-specific implant-bone geometry. OPENSIM inverse kinematics, inverse dynamics, and muscle analyses were performed to calculate joint kinematics, joint moments, and muscle-tendon lengths, velocities, and moment arms for the selected gait cycle, normalized to 101 time frames.

In preparation for estimating muscle forces via optimization and joint stiffnesses via analytical calculations, we developed surrogate models of the OPENSIM musculoskeletal geometry. The surrogate models were based on a cubic polynomial fit of muscle-tendon length as a function of involved generalized coordinates [13,38,48]. For each muscle, a linear least squares solution was performed to find a single set of polynomial coefficients that fitted muscle-tendon length and associated moment arms simultaneously as a function of spanned joint angles. For example, for a uniarticular muscle i crossing a single joint j possessing generalized coordinate θ_j, muscle-tendon length ℓ_i^{MT} and moment arm r_{ij} were fitted simultaneously assuming [13,49]

$$\begin{aligned} \ell_i^{MT} &= b_0 + b_1\theta_j + b_2\theta_j^2 + b_3\theta_j^3 \\ r_{ij} &= -\frac{\partial \ell_i^{MT}}{\partial \theta_j} = -b_1 - 2b_2\theta_j - 3b_3\theta_j^2 \end{aligned} \tag{1}$$

Muscle-tendon velocity was then defined analytically using the same polynomial coefficients

$$v_i^{MT} = \frac{d\ell_i^{MT}}{dt} = b_1\dot{\theta}_j + 2b_2\theta_j\dot{\theta}_j + 3b_3\theta_j^2\dot{\theta}_j \tag{2}$$

This approach was extended to muscles spanning multiple joints.

Optimization Formulations. Two optimization formulations were implemented in MATLAB [50] using a custom Hill-type muscle model with rigid tendon, which is a reasonable assumption for walking [7,8]. Muscle-tendon model parameter values were taken from Ref. [39]. Tendon force F_i^T produced by each Hill-type muscle i was formulated as [51]

$$F_i^T = F_{oi}^M\left[f_\ell\left(\tilde{\ell}_i^M\right)f_v\left(\tilde{v}_i^M\right)a_i + f_p\left(\tilde{\ell}_i^M\right)\right]\cos\alpha_i \tag{3}$$

where F_{oi}^M is the peak isometric force, $f_\ell\left(\tilde{\ell}_i^M\right)$ is the normalized active force–length relationship, $f_v(\tilde{v}_i^M)$ is the normalized active force–velocity relationship, a_i is the activation, $f_p\left(\tilde{\ell}_i^M\right)$ is the normalized passive force–length relationship, and α_i is the pennation angle. Normalized force-length and force-velocity curves were defined by smooth analytical functions to facilitate formation of analytical derivatives for joint stiffness calculations. For both optimization formulations, no reserve actuators or activation dynamics were used, and errors in inverse dynamic joint moment matching were quantified using root-mean-square (RMS) and R^2 metrics.

The first optimization formulation was SO. Since muscle activations were independent between time frames, the optimization problem was solved one time frame at a time. The static optimization problem used muscle activations as design variables and was formulated as in Ref. [20]

$$\begin{aligned} &\min_{a_i} \sum_{i=1}^{44} a_i^2 \\ &\text{subject to} \\ &M_j = \sum_{i=1}^{44} r_{ij}F_i^T \ (j = 1, \ldots, 6) \\ &0 \le a_i \le 1 \ (i = 1, \ldots, 44) \end{aligned} \tag{4}$$

where a_i is the activation of muscle i, M_j is the inverse dynamics moment for joint j, r_{ij} is the moment arm of muscle i about joint j, and F_i^T is the tendon force for muscle i, all at the current time frame. For computational efficiency, since the moment matching constraint in Eq. (4) is a linear function of the design variables a_i, we implemented the SO formulation as a quadratic programming problem and solved it using MATLAB's *quadprog* optimization algorithm.

The second optimization formulation was our synergy-based formulation (SynO). In this formulation, a synergy structure was imposed on the muscle activations by design. Since synergy vector weights were time-invariant across time frames, this optimization problem was solved over all time frames simultaneously. Construction of synergy-based muscle activations was inspired by non-negative matrix factorization [52–56]

$$a_i(t) = \sum_{p=1}^{n} w_{ip} s_p(t) \; (i = 1, \ldots, 44) \tag{5}$$

where $a_i(t)$ is the activation of muscle i as a function of time, w_{ip} is the time-invariant synergy vector weight for muscle i and synergy p ($w_{ip} \geq 0$), and $s_p(t)$ is the time-varying synergy activation for synergy p as a function of time ($s_p(t) \geq 0$). To make the synergy solution unique, we required the sum of all weights in each synergy vector to equal 1

$$\sum_{i=1}^{44} w_{ip} = 1 \; (p = 1, \ldots, n) \tag{6}$$

where each synergy vector specifies intermuscle activation coupling. Furthermore, to reduce the number of design variables required to construct all muscle activations over all time frames, we parameterized each time-varying synergy activation $s_p(t)$ using a B-spline function constructed from 21 adjustable nodal points spanning the gait cycle

$$s_p(t) = \sum_{l=1}^{21} f(b_{lp}, t) \tag{7}$$

where b_{lp} is nodal point l for synergy p. The complete optimization problem was formulated as

$$\min_{w_{ip}, b_{lp}} \sum_{k=1}^{101} \left(\sum_{i=1}^{44} a_{ik}^2 + \sum_{j=1}^{6} \left(M_{jk} - \sum_{i=1}^{44} r_{ijk} F_{ik} \right)^2 \right)$$

subject to

$$\sum_{i=1}^{44} w_{ip} = 1 \; (p = 1, \ldots, n)$$

$$w_{ip} \geq 0, b_{lp} \geq 0 \tag{8}$$

where

$$a_{ik} = \sum_{p=1}^{n} w_{ip} s_{pk}$$

$$s_{pk} = f(b_{lp}, k) \; (l = 1, \ldots, 21)$$

where k indicates the time frame being evaluated, w_{ip} ($i = 1, \ldots, 44$) and b_{lp} ($l = 1, \ldots, 21$) are the design variables, and n indicates the selected number of synergies to use for constructing muscle activations. In this formulation, joint moment tracking was included in the cost function rather than the constraints since a limited number of activation synergies will never be able to match the inverse dynamic joint moments perfectly. We implemented our SynO formulation as a nonlinear programming problem with linear equality constraints and solved it using MATLAB's *fmincon* optimization algorithm.

Compared to the SO formulation, SynO theoretically (though not practically) eliminates the muscle force indeterminacy problem, as shown by considering the number of equations and number of unknowns in both formulations. For SO, each time frame possesses six equations from inverse dynamic joint moment matching and 44 unknown muscle activations, creating a highly underdetermined problem. In contrast, for our SynO formulation, the complete gait cycle possesses six joint moments $\times$ 101 time frames $= 606$ equations from inverse dynamic joint moment matching and n synergies $\times$ (44 synergy vector weights/synergy $+ 21$ B-spline nodal points/synergy) $= n \times 65$ unknowns for activation construction. The number of unknowns for 2–6 synergies is therefore

$$\begin{aligned} Unknowns &= n \times 65 \\ &= 130 \; (n = 2) \\ &= 195 \; (n = 3) \\ &= 260 \; (n = 4) \\ &= 325 \; (n = 5) \\ &= 390 \; (n = 6) \end{aligned} \tag{9}$$

Thus, even for six synergies, the muscle force solution is theoretically overdetermined with 606 equations and 390 unknowns. However, in practice, since neighboring time frames are not completely independent from one another, the solutions remain underdetermined, necessitating the inclusion of an activation minimization term (also called a regularization term [57]) in the cost function.

Joint Stiffness Calculation. For all muscle force solutions, the total stiffness of each lower body joint at each time frame was calculated using analytical relationships derived from our rigid-tendon Hill-type muscle model and surrogate musculoskeletal geometry. In brief, for any joint j possessing generalized coordinate θ_j and joint moment M_j, joint stiffness k_j due to the active and passive force-length properties of all muscles spanning the joint was defined as

$$k_j = -\frac{\partial M_j}{\partial \theta_j} \quad \text{where} \quad M_j = \sum_{i=1}^{44} r_{ij} F_i^T \tag{10}$$

Carrying out the partial derivative and employing the chain rule for differentiation leads to

$$k_j = -\sum_{i=1}^{n} \left(\frac{\partial r_{ij}}{\partial \theta_j} F_i^T + r_{ij} \frac{\partial F_i^T}{\partial \ell_i^{MT}} \frac{\partial \ell_i^{MT}}{\partial \theta_j} \right) \tag{11}$$

Recalling the relationship between r_{ij} and ℓ_i^{MT} (review Eq. (1)), Eq. (11) simplifies further to

$$k_j = -\sum_{i=1}^{n} \left(\frac{\partial r_{ij}}{\partial \theta_j} F_i^T - r_{ij}^2 \frac{\partial F_i^T}{\partial \ell_i^{MT}} \right) \tag{12}$$

The two remaining partial derivatives in Eq. (12) were formed analytically, the first from Eq. (1), and the second from Eq. (3). Analytic calculation of the second partial derivative would not have been possible if a compliant tendon model had been used. Thus, for slow activities such as walking where a rigid tendon model is justifiable [7,8], Eq. (12) makes it possible to calculate joint stiffness analytically given muscle activations and joint kinematics.

Results

Joint Moment Matching. All six lower extremity joint moments were matched well by both SynO and SO (Table 1, Fig. 1), despite the omission of reserve actuators from the optimization problem formulations. SO matched inverse dynamic joint moments to within the specified constraint tolerance of 1×10^{-6}. SynO matched inverse dynamic joint moments with increasing fidelity, as indicated by decreasing RMS errors and increasing R^2 values (see Table 1), as the number of synergies was increased. The worst SynO joint moment matching (especially for the hip rotation moment) was produced for two synergies. By four synergies, all RMS errors were less than 1 N·m and all R^2 values were

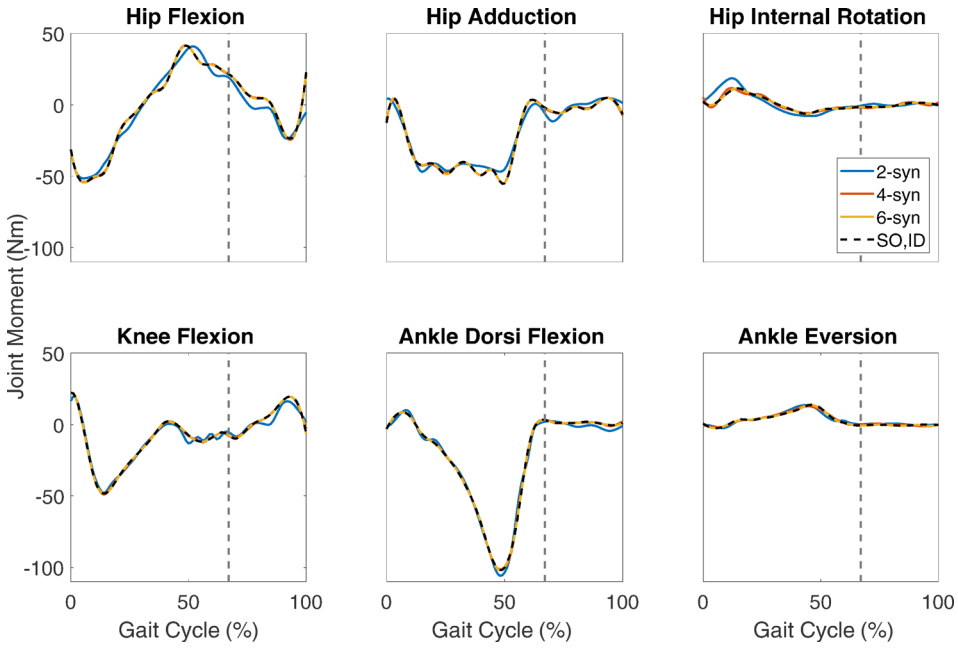

Fig. 1 Net joint moments matching results over the gait cycle for inverse dynamics (ID; black) and synergy optimization with 2 (blue), 4 (red), and 6 (yellow) synergies. SO moments were identical to those of ID to the numerical tolerance of 1×10^{-6}. Plot titles refer to positive direction. The gait cycle is defined from heel strike to subsequent heel strike of the right leg. Dashed gray lines indicate right toe-off.

Table 1 RMS errors (first row, N·m) and R^2 values (second row) for inverse dynamic joint moment matching using the SynO approach

Number of synergies	Hip flexion	Hip adduction	Hip rotation	Knee flexion	Ankle flexion	Ankle inversion
2	5.4	4.2	3.4	2.6	2.5	1.1
	0.96	0.96	0.39	0.98	0.99	0.94
3	1.5	2.2	1.6	1.5	2.0	1.0
	1.00	0.99	0.86	0.99	1.00	0.95
4	0.4	0.5	0.9	0.5	0.6	0.7
	1.00	1.00	0.95	1.00	1.00	0.98
5	0.2	0.3	0.3	0.2	0.3	0.7
	1.00	1.00	0.99	1.00	1.00	0.98
6	0.2	0.1	0.1	0.2	0.2	0.3
	1.00	1.00	1.00	1.00	1.00	1.00

0.95 or higher. By six synergies, the SynO joint moment solutions became visually indistinguishable from those produced by SO.

Muscle Activation Estimation. In contrast to the joint moment results, the muscle activation results were visibly different between the SynO and SO solutions (Fig. 2). For some muscles, the activations estimated by SynO were insensitive to the number of synergies (e.g., glmin2), while for other muscles, the estimated activations were highly sensitive and decreased as the number of synergies increased (e.g., gaslat) (Fig. 2). Sensitive muscles tended to be those that spanned the hip and/or knee. For two synergies, the activations of several muscles (e.g., bfsh, gaslat, glmin1) went well above 1, as no upper bound on muscle activations was used in the SynO formulation. In general, as the number of synergies approached six, muscle activations estimated by SynO approached those estimated by SO (Fig. 2).

Joint Stiffness Estimation. Also, in contrast to the joint moment results, the joint stiffness results were visibly different between the SynO and SO solutions (Figs. 3 and 4). During stance phase, joint stiffness for hip flexion and knee flexion, but not for the other joints, was affected by the selected number of synergies, with stiffness decreasing as the number of synergies was increased. By six synergies, the stiffness of each joint was low and approximately constant, becoming essentially the same as that produced by SO. In contrast, during swing phase, joint stiffness was low and approximately constant regardless of how the optimization was performed.

Discussion

This study explored how a modified static optimization method that imposed a synergy structure on estimated muscle activations affected calculated lower body joint stiffnesses during walking. Although SynO finds synergy activations over all time frames simultaneously, it is still a static optimization approach because it uses algebraic rather than differential equations [58]. To compare SynO to SO, we used walking data taken by the First Grand Challenge Competition to Predict in vivo Knee Loads [46]. We found that while joint moment matching was relatively insensitive to the selected number of synergies, joint stiffnesses associated with hip and knee flexion were highly sensitive, with peak values decreasing as the number of synergies was increased. Reasonable joint moment matching could be achieved with a low number of

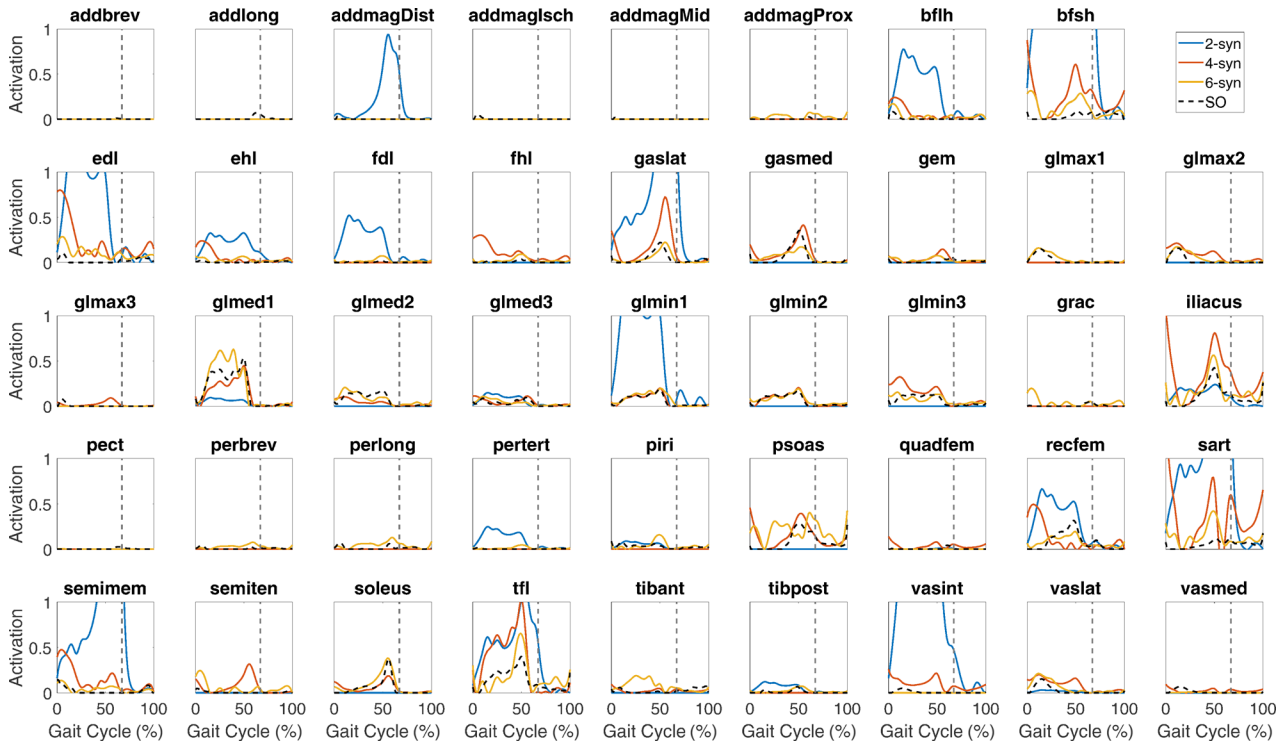

Fig. 2 Muscle activation results for SO (black) and synergy optimization with 2 (blue), 4 (red), and 6 (yellow) synergies. Dashed gray lines indicate right toe-off. Muscle labels are adductor brevis (addbrev), adductor longus (addlong), adductor magnus proximal (addmagProx), adductor magnus middle (addmagMid), adductor magnus distal (addmagDist), adductor magnus ischial (addmagIsch), biceps femoris long head (bflh), biceps femoris short head (bfsh), extensor digitorum longus (edl), extensor hallucis longus (ehl), flexor digitorum longus (fdl), flexor hallucis longus (fhl), lateral gastrocnemius (gaslat), medial gastrocnemius (gasmed), gemellus (gem), gluteus maximus (glmax1, glmax2, glmax3), gluteus medius (glmed1, glmed2, glmed3), gluteus minimus (glmin1, glmin2, glmin3), gracilis (grac), iliacus, pectoralis (pect), peroneus brevis (perbrev), peroneus longus (perlong), peroneus tertius (pertert), piriformis (piri), psoas, quadratus femoris (quadfem), rectus femoris (recfem), sartorius (sart), semimembranosus (semimem), semitendinosus (semiten), soleus, tensor fasciae latae (tfl), tibialis anterior (tibant), tibialis posterior (tibpost), vastus intermedius (vasint), vastus lateralis (vaslat), and vastus medialis (vasmed).

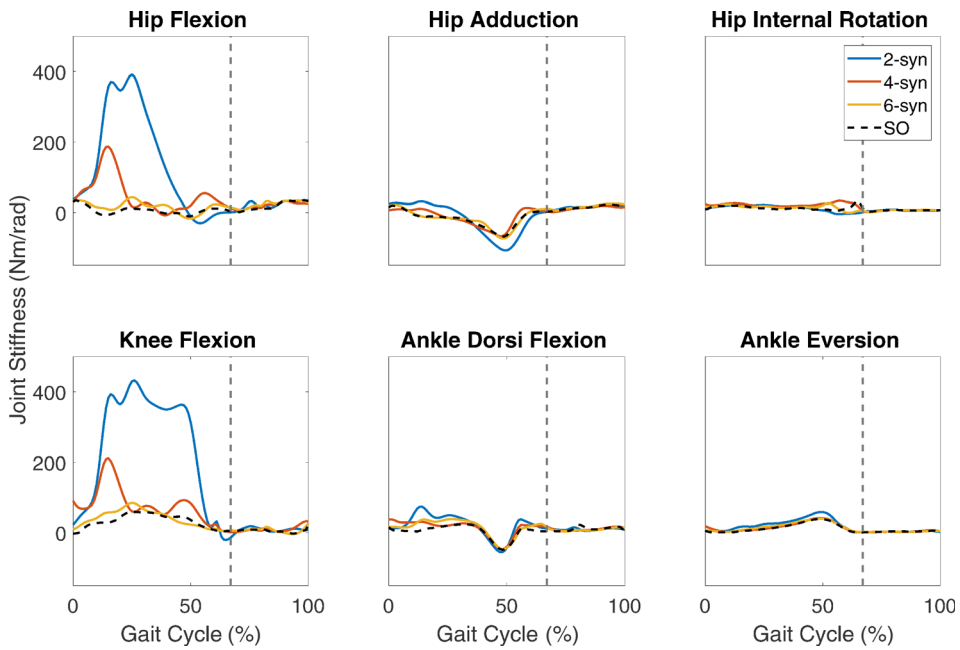

Fig. 3 Joint stiffness results over the gait cycle for SO (black) and synergy optimization with 2 (blue), 4 (red), and 6 (yellow) synergies. The gait cycle is defined from heel strike to subsequent heel strike of the right leg. Dashed gray lines indicate right toe-off.

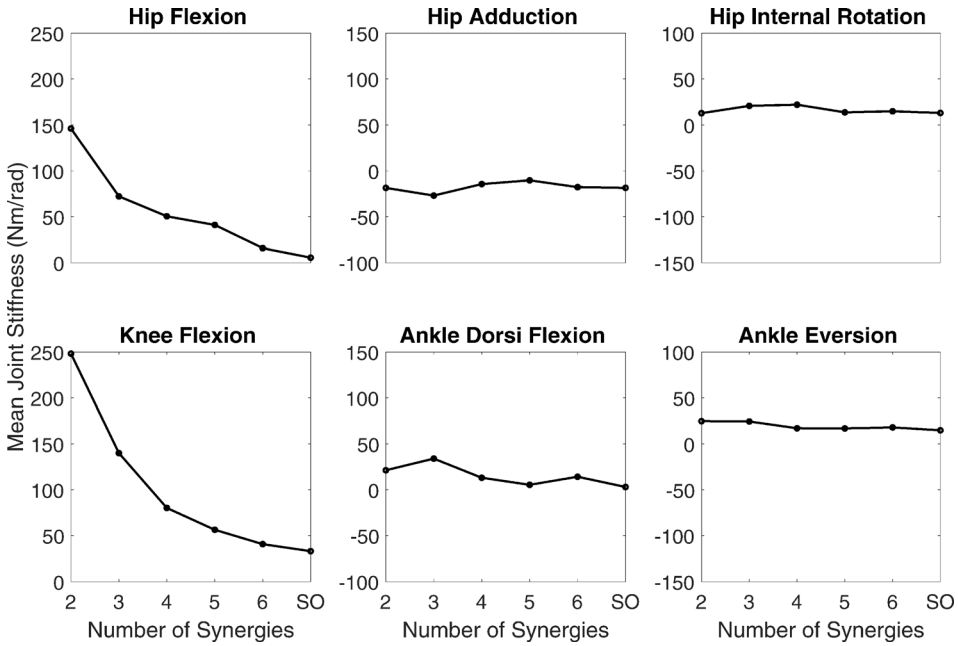

Fig. 4 Mean joint stiffness over stance phase for SO and synergy optimization with 2–6 synergies. The gait cycle is defined from heel strike to subsequent heel strike of the right leg.

synergies by increasing the activations in only a subset of muscles, which in turn necessitated increased antagonistic muscle activations and ultimately increased joint stiffnesses. This finding might have important implications for stroke neurorehabilitation, where a stroke often results in a decreased number of paretic leg synergies [59], which could potentially increase hip and knee stiffness.

The synergy optimization method used in this study is similar to the method presented in Ref. [36], which also optimized synergy vector weights and synergy activations simultaneously. However, our SynO approach was different in three ways. First, we used a different muscle model. Whereas Gopalakrishnan et al. [36] used a Hill-type muscle model with a compliant tendon, our study used a Hill-type muscle model with a rigid tendon that allowed us to analytically calculate individual muscle contributions to the stiffness of spanned joints. Second, we used a different approach for calculating muscle forces. Whereas the compliant tendon model used in Ref. [36] required numerical integration of first-order ordinary differential equations to calculate muscle force time histories, our rigid tendon model allowed muscle forces to be calculated algebraically at each time point. Third, we used a different approach for solving the optimization problem across all time frames simultaneously. Whereas Gopalakrishnan et al. [36] used direct collocation optimal control with a separate design variable defining each synergy control at each time instant, we defined each synergy control using 21 B-spline nodes, which significantly reduced the number of design variables and made the solution closer to determinate. The net result of these three differences was lower computation time for SynO over the direct collocation approach used in Ref. [36]. For six synergies, SynO required 6–8 min of CPU time to converge from random initial guesses, and only 2–4 min for four synergies. In Ref. [36], a solution using four synergies required 10–20 min of CPU time, which is not surprising given the added computational cost of repeated numerical integration. Our simulations were performed on a computer with an Intel Xeon Gold 6144 processor, 3.50 GHz CPU, and 128 GB of RAM. Computer specifications were not reported in Ref. [36].

Imposing a muscle synergy structure on estimated muscle activations leads to several advantages compared to SO. One advantage is that muscle activation discontinuities between time frames may be largely eliminated due to a lower number of time-varying controls that each affects the activation of multiple muscles. Another advantage is that the level of indeterminacy in the muscle force solution is reduced due to the reduced number of design variables provided by a synergy structure. A third advantage is that it may be easier to identify subject-specific neural control characteristics due to the greater uniqueness provided by a synergy structure, especially if the number of synergies is defined based on analysis of the subject's experimental EMG data. A fourth advantage is the ability to incorporate joint stiffness considerations into new optimization methods for estimating muscle forces. However, the advantages of SynO over SO come at the cost of a more computationally expensive and complex optimization process, since use of time-invariant synergy vector weights as design variables requires that all time frames be solved simultaneously.

This study also presented an analytical joint stiffness formula for estimating the total stiffness due to active and passive force-length properties of all muscles spanning a joint. An analytical derivation of joint stiffness was possible due to the rigid tendon assumption in the musculotendon model and surrogate model fitting of muscle-tendon lengths and moment arms. This analytical stiffness formula may be useful for many different human-centered applications, such as in biomechanics, rehabilitation, and human–robot interaction. The central nervous system regulates joint stiffnesses as well as joint moments during human movement [26,27], for example, for controlling stability or absorbing impacts during gait [26], or for stabilizing movements in unstable environments [60] or unpredictable situations [61]. Therefore, analytical joint stiffness calculations could facilitate the development of novel optimization cost functions and/or constraints that produce more reliable muscle force estimates. In rehabilitation, since excessive joint stiffness can impair movement ability [62], analytical joint stiffness calculations could be used to facilitate identification of alternate neural control strategies that maximize recovery of lost function. Since impedance control is frequently used in robotics, analytical joint stiffness calculations could also be useful for the design of more robust controllers in human–robot interaction applications [63].

An interesting finding was that SO produced the lowest muscle activation and joint stiffness results compared to all of the SynO results. This finding is likely due to the fact that SO minimizes antagonistic muscle activations, as previously reported [23,24]. In contrast, our SynO approach constrains muscles to act within synergy groups, using B-splines to ensure the continuity of each time-varying synergy activation. The imposed synergy structure leads to higher levels of antagonistic activation, potentially resolving a shortcoming in static optimization. However, the new dilemma becomes how to choose the correct number of synergies for any particular subject.

Among the six joints in our OPENSIM model, joint stiffness estimates for hip adduction and ankle dorsiflexion were consistently negative at the midpoint of the gait cycle (Fig. 3), which would suggest a destabilizing effect on the motion [64]. There are two possible interpretations for this finding. The first is that the finding is correct and has some rational explanation. These negative stiffness regions occur at the maximum value of the anterior ground reaction force. At the same time point, the hip begins a rapid shift toward maximum abduction and the ankle toward maximum plantarflexion at toe-off (dashed gray line). Negative stiffness might facilitate further movement of both joints in the direction of the motion, rather than resistance in that direction [25]. In this case, such an effect would either place the foot back on the ground or accelerate the push-off and unloading process that initiates swing phase while maintaining forward progression. Thus, this small region of negative stiffness may help ensure that the transition from stance to swing phase is either completed successfully or not completed safely. The second possible interpretation is that the finding is incorrect and reflects small errors in the model structure, model parameter values, and/or experimental inputs. Either way, these negative dips are small compared to the maximum hip flexion and knee flexion stiffness estimated during stance phase for low numbers of synergies. Whether these small regions of negative stiffness are correct, common, or biomechanically helpful will require further research.

While it is difficult to explain the possible biomechanical significance of small negative joint stiffnesses, it is not difficult to calculate which muscles contribute to them, and why. An advantage of our analytical joint stiffness formula is that it makes such calculations possible. Our joint stiffness formula (Eq. (12)) contains two terms: $-(\partial r_{ij}/\partial\theta_j)F_i^T$ and $r_{ij}^2(\partial F_i^T/\partial\ell_i^{MT})$. For negative stiffness to occur, the sum of these two terms must be negative. Since F_i^T is always non-negative, the first term will be negative when $\partial r_{ij}/\partial\theta_j$ is positive. Thus, a negative muscle contribution to joint stiffness can occur when an increase in generalized coordinate value produces an increase in moment arm value. Since r_{ij}^2 is always positive, the second term will be negative when $\partial F_i^T/\partial\ell_i^{MT}$ is negative. Thus, a negative muscle contribution to joint stiffness can also occur when an increase in muscle-tendon length produces a decrease in tendon force, which is possible when a muscle's normalized fiber length is greater than 1.

Following this approach, we were able to identify which muscles were the primary contributors to negative joint stiffness, and why the negative values occurred. For negative hip adduction stiffness, iliacus, sartorius, rectus femoris, and tensor fascia latae were the primary contributors, while for negative ankle flexion stiffness, gastrocnemius medialis, gastrocnemius lateralis, and soleus were the key muscles. For all of these muscles, negative stiffness was caused primarily by the first term in our stiffness formula through a combination of a positive $\partial r_{ij}/\partial\theta_j$ value and a large F_i^T value.

Depending on the environment and cognitive situation, humans modulate joint stiffness during gait to control stability or absorb impacts [26]. One might walk in a relaxed manner with minimum joint stiffness, or one might walk in a rigid manner with higher joint stiffness. Antagonistic muscles can be recruited to increase joint stiffness while keeping the net muscle moment the same. This possibility implies that in addition to matching joint moments, which is a requirement of dynamic equilibrium, the central nervous system adjusts muscle forces to modulate joint stiffness [65], which could occur through changes in reflex behavior [66] or activation-dependent alterations in muscle properties [67,68].

Some researchers have suggested that individuals with neurological disorders such as stroke or Parkinson's disease walk with increased joint stiffness, potentially to maintain greater stability and reject walking disturbances [69,70]. Individuals with these disorders have also been shown to use a lower number of muscle synergies than do healthy individuals [59,71]. Our study suggests that these two observations may be related, with increased joint stiffness being required to achieve specified inverse dynamic joint moments using a low number of synergies. Further exploration of this issue should be performed by analyzing walking data collected from individuals with neurological disorders.

Although activation minimization has historically been used to solve the muscle redundancy problem, this cost function minimizes antagonistic co-activation and therefore joint stiffness. Given that the body modulates joint stiffness during movement [26], quantification of joint stiffness using experimental measurements and neuromusculoskeletal models may eventually lead to more realistic estimates of antagonistic muscle co-activation.

This study possessed a number of limitations that should be considered when evaluating our results. First, subject-specific neural control factors were not modeled. Rather, our muscle activation and force estimates were generated solely using optimization methods without assistance from EMG data. Validation of the estimated activations against EMG measurements would be a future study. Second, activation dynamics was omitted. Activation dynamics limits how fast muscle activations can vary, which could potentially alter our results. Third, only a single gait cycle from a single subject was analyzed. Future plans include analyzing gait data from a larger number of subjects and trials. Fourth, the subject analyzed was not neurologically impaired in any obvious way. Studying impaired subjects (e.g., due to stroke or spinal cord injury) using the number of synergies identified in their EMG data would be beneficial for evaluating our SynO approach as well as joint stiffness differences between subjects. Fifth, no joint stiffness measurements exist for this subject that could be used for validation purposes. Though joint stiffness is difficult to measure experimentally under dynamic functional conditions [72], such stiffness measurements during walking could significantly improve our ability to estimate muscle forces reliably. Sixth, joint stiffness depends on musculoskeletal geometry and musculotendon model parameter values, and only a single set of parameter values was used in this study, as obtained from Ref. [39]. A thorough sensitivity analysis to investigate how variations in relevant model parameter values affect total joint stiffness would be worthwhile.

In conclusion, this study demonstrated how imposition of a synergy structure on the muscle activations found via optimization affects the stiffness of lower body joints during walking. We found that inverse dynamic joint moment matching improved little as the number of synergies is increased from 2 to 6. We also found that hip and knee joint stiffness during stance phase decreased substantially as the number of synergies was increased from 2 to 6, with static optimization producing the lowest stiffness of all joints. Although it had been previously reported that static optimization minimizes antagonistic cocontraction, no study to our knowledge had investigated the connection between SO and joint stiffness. In terms of clinical relevance, this study suggests that individuals with neurological disorders may walk with a stiff gait pattern due to a reduced number of muscle synergies. This hypothesis could be tested using gait data collected from subjects with stroke or Parkinson's disease.

Acknowledgment

This work was funded by the Cancer Prevention and Research Institute of Texas (CPRIT) under grant RR170026.

References

[1] Erdemir, A., McLean, S., Herzog, W., and van den Bogert, A. J., 2007, "Model-Based Estimation of Muscle Forces Exerted During Movements," Clin. Biomech., **22**(2), pp. 131–154.

[2] Anderson, F. C., and Pandy, M. G., 1999, "A Dynamic Optimization Solution for Vertical Jumping in Three Dimensions," Comput. Methods Biomech. Biomed. Eng., **2**(3), pp. 201–231.

[3] Ackermann, M., and van den Bogert, A. J., 2010, "Optimality Principles for Model-Based Prediction of Human Gait," J. Biomech., **43**(6), pp. 1055–1060.

[4] Shourijeh, M. S., and McPhee, J., 2014, "Forward Dynamic Optimization of Human Gait Simulations: A Global Parameterization Approach," ASME J. Comput. Nonlinear Dyn, **9**(3), p. 31018.

[5] Ackermann, M., and Schiehlen, W., 2009, "Physiological Methods to Solve the Force-Sharing Problem in Biomechanics," *Multibody Dynamics*, Vol. 12, C. Bottasso, ed., Springer, Dordrecht, The Netherlands, pp. 1–23.

[6] Shourijeh, M. S., Mehrabi, N., and McPhee, J., 2017, "Forward Static Optimization in Dynamic Simulation of Human Musculoskeletal Systems: A Proof-of-Concept Study," ASME J. Comput. Nonlinear Dyn., **12**(5), p. 051005.

[7] Anderson, F. C., and Pandy, M. G., 2001, "Static and Dynamic Optimization Solutions for Gait Are Practically Equivalent," J. Biomech., **34**(2), pp. 153–161.

[8] De Groote, F., Kinney, A. L., Rao, A. V., and Fregly, B. J., 2016, "Evaluation of Direct Collocation Optimal Control Problem Formulations for Solving the Muscle Redundancy Problem," Ann. Biomed. Eng., **44**(10), pp. 2922–2936.

[9] Hof, A. L., and den Berg, J., 1981, "EMG to Force Processing II: Estimation of parameters of the Hill Muscle Model for the Human Triceps Surae by Means of a Calfergometer," J. Biomech., **14**(11), pp. 759–770.

[10] Lloyd, D. G., and Besier, T. F., 2003, "An EMG-Driven Musculoskeletal Model to Estimate Muscle Forces and Knee Joint Moments In Vivo," J. Biomech., **36**(6), pp. 765–776.

[11] Buchanan, T. S., Lloyd, D. G., and Manal, K., 2004, "Neuromusculoskeletal Modeling : Estimation of Muscle Forces and Joint Moments and Movements From Measurements of Neural Command," J. Appl. Biomech., **20**(4), pp. 367–395.

[12] Sartori, M., Reggiani, M., Farina, D., and Lloyd, D. G., 2012, "EMG-Driven Forward-Dynamic Estimation of Muscle Force and Joint Moment About Multiple Degrees of Freedom in the Human Lower Extremity," PLoS One, **7**(12), p. e52618.

[13] Meyer, A. J., and Fregly, B. J., 2016, "Lower Extremity EMG-Driven Modeling With Automated Adjustment of Geometry," PLoS One, **12**(7), p. e0179698.

[14] Farina, D., Merletti, R., and Enoka, R. M., 2004, "The Extraction of Neural Strategies From the Surface EMG," J. Appl. Physiol., **96**(4), pp. 1486–1495.

[15] Winter, D. A., Fuglevand, A. J., and Archer, S. E., 1994, "Crosstalk in Surface Electromyography: Theoretical and Practical Estimates," J. Electromyogr. Kinesiol., **4**(1), pp. 15–26.

[16] De Luca, C. J., Gilmore, L. D., Kuznetsov, M., and Roy, S. H., 2010, "Filtering the Surface EMG Signal: Movement Artifact and Baseline Noise Contamination," J. Biomech., **43**(8), pp. 1573–1579.

[17] Fridlund, A. J., and Cacioppo, J. T., 1986, "Guidelines for Human Electromyographic Research," Psychophysiology, **23**(5), pp. 567–589.

[18] Mirka, G. A., 1991, "The Quantification of EMG Normalization Error," Ergonomics, **34**(3), pp. 343–352.

[19] S. Shourijeh, M., Smale, K. B., Potvin, B. M., and Benoit, D. L., 2016, "A Forward-Muscular Inverse-Skeletal Dynamics Framework for Human Musculoskeletal Simulations," J. Biomech., **49**(9), pp. 1718–1723.

[20] Happee, R., and Van der Helm, F. C. T., 1995, "The Control of Shoulder Muscles During Goal-Directed Movements, an Inverse Dynamic Analysis," J. Biomech., **28**(10), pp. 1179–1191.

[21] Shourijeh, M. S., and McPhee, J., 2014, "Optimal Control and Forward Dynamics of Human Periodic Motions Using Fourier Series for Muscle Excitation Patterns," ASME J. Comput. Nonlinear Dyn., **9**(2), p. 021005.

[22] Delp, S. L., Anderson, F. C., Arnold, A. S., Loan, P., Habib, A., John, C. T., Guendelman, E., and Thelen, D. G., 2007, "OpenSim: Open Source to Create and Analyze Dynamic Simulations of Movement," IEEE Trans. Biomed. Eng., **54**(11), pp. 1940–1950.

[23] Herzog, W., and Binding, P., 1992, "Predictions of Antagonistic Muscular Activity Using Nonlinear Optimization," Math. Biosci., **111**(2), pp. 217–229.

[24] Herzog, W., and Binding, P., 1993, "Cocontraction of Pairs of Antagonistic Muscles: Analytical Solution for Planar Static Nonlinear Optimization Approaches," Math. Biosci., **118**(1), pp. 83–95.

[25] Davis, R. B., and DeLuca, P. A., 1996, "Gait Characterization Via Dynamic Joint Stiffness," Gait Posture, **4**(3), pp. 224–231.

[26] Pfeifer, S., Vallery, H., Hardegger, M., Riener, R., and Perreault, E. J., 2012, "Model-Based Estimation of Knee Stiffness," IEEE Trans. Biomed. Eng., **59**(9), pp. 2604–2612.

[27] Sartori, M., Maculan, M., Pizzolato, C., Reggiani, M., and Farina, D., 2015, "Modeling and Simulating the Neuromuscular Mechanisms Regulating Ankle and Knee Joint Stiffness During Human Locomotion," J. Neurophysiol., **114**(4), pp. 2509–2527.

[28] Neptune, R. R., Clark, D. J., and Kautz, S. A., 2009, "Modular Control of Human Walking: A Simulation Study," J. Biomech., **42**(9), pp. 1282–1287.

[29] Allen, J. L., and Neptune, R. R., 2012, "Three-Dimensional Modular Control of Human Walking," J. Biomech., **45**(12), pp. 2157–2163.

[30] Razavian, R. S., Ghannadi, B., and McPhee, J., 2019, "A Synergy-Based Motor Control Framework for the Fast Feedback Control of Musculoskeletal Systems," ASME J. Biomech. Eng., **141**(3), p. 031009.

[31] Mehrabi, N., Schwartz, M. H., and Steele, K. M., 2019, "Can Altered Muscle Synergies Control Unimpaired Gait?," J. Biomech., **90**, pp. 84–91.

[32] Allen, J. L., Kautz, S. A., and Neptune, R. R., 2013, "The Influence of Merged Muscle Excitation Modules on Post-Stroke Hemiparetic Walking Performance," Clin. Biomech., **28**(6), pp. 697–704.

[33] McGowan, C. P., Neptune, R. R., Clark, D. J., and Kautz, S. A., 2010, "Modular Control of Human Walking: Adaptations to Altered Mechanical Demands," J. Biomech., **43**(3), pp. 412–419.

[34] Sartori, M., Gizzi, L., Lloyd, D. G., and Farina, D., 2013, "A Musculoskeletal Model of Human Locomotion Driven by a Low Dimensional Set of Impulsive Excitation Primitives," Front. Comput. Neurosci., **7**, pp. 1–22.

[35] Walter Allison, J. P., Kinney, L., Banks, S. A., D'Lima, D. D., Besier, T. F., Lloyd, D. G., and Fregly, B. J., 2014, "Muscle Synergies May Improve Optimization Prediction of Knee Contact Forces During Walking," ASME J. Biomech. Eng, **136**(2), p. 21031.

[36] Gopalakrishnan, A., Modenese, L., and Phillips, A. T. M., 2014, "A Novel Computational Framework for Deducing Muscle Synergies From Experimental Joint Moments," Front. Comput. Neurosci., **8**, pp. 1–15.

[37] Steele, K. M., Tresch, M. C., and Perreault, E. J., 2015, "Consequences of Biomechanically Constrained Tasks in the Design and Interpretation of Synergy Analyses," J. Neurophysiol., **113**(7), pp. 2102–2113.

[38] Meyer, A. J., Eskinazi, I., Jackson, J. N., Rao, A. V., Patten, C., and Fregly, B. J., 2016, "Muscle Synergies Facilitate Computational Prediction of Subject-Specific Walking Motions," Front. Bioeng. Biotechnol., **4**(77), pp. 1–26.

[39] Serrancolí, G., Kinney, A. L., Fregly, B. J., and Font-Llagunes, J. M., 2016, "Neuromusculoskeletal Model Calibration Significantly Affects Predicted Knee Contact Forces for Walking," ASME J. Biomech. Eng, **138**(8), p. 81001.

[40] Ivanenko, Y. P., Poppele, R. E., and Lacquaniti, F., 2004, "Five Basic Muscle Activation Patterns Account for Muscle Activity During Human Locomotion," J. Physiol., **556**(1), pp. 267–282.

[41] Cappellini, G., Ivanenko, Y. P., Poppele, R. E., and Lacquaniti, F., 2006, "Motor Patterns in Human Walking and running," J. Neurophysiol., **95**(6), pp. 3426–3437.

[42] Shourijeh, M. S., Flaxman, T. E., and Benoit, D. L., 2016, "An Approach for Improving Repeatability and Reliability of Non-Negative Matrix Factorization for Muscle Synergy Analysis," J. Electromyogr. Kinesiol., **26**, pp. 36–43.

[43] Bianco, N. A., Patten, C., and Fregly, B. J., 2018, "Can Measured Synergy Excitations Accurately Construct Unmeasured Muscle Excitations?," ASME J. Biomech. Eng, **140**(1), p. 011011.

[44] Smale, K. B., Shourijeh, M. S., and Benoit, D. L., 2016, "Use of Muscle Synergies and Wavelet Transforms to Identify Fatigue During Squatting," J. Electromyogr. Kinesiol., **28**, pp. 158–166.

[45] Kristiansen, M., Madeleine, P., Hansen, E. A., and Samani, A., 2014, "Inter-Subject Variability of Muscle Synergies During Bench Press in Power Lifters and Untrained Individuals," Scand. J. Med. Sci. Sports, **25**(1), pp. 89–97.

[46] Fregly, B. J., Besier, T. F., Lloyd, D. G., Delp, S. L., Banks, S. A., Pandy, M. G., and D'Lima, D. D., 2012, "Grand Challenge Competition to Predict In Vivo Knee Loads," J. Orthop. Res., **30**(4), pp. 503–513.

[47] Arnold, E. M., Ward, S. R., Lieber, R. L., and Delp, S. L., 2010, "A Model of the Lower Limb for Analysis of Human Movement," Ann. Biomed. Eng., **38**(2), pp. 269–279.

[48] Menegaldo, L. L., de Toledo Fleury, A., and Weber, H. I., 2004, "Moment Arms and Musculotendon Lengths Estimation for a Three-Dimensional Lower-Limb Model," J. Biomech., **37**(9), pp. 1447–1453.

[49] Sherman, M. A., Seth, A., and Delp, S. L., 2013, "What Is a Moment Arm? Calculating Muscle Effectiveness in Biomechanical Models Using Generalized Coordinates," ASME Paper No. DETC2013-13633.

[50] MATLAB, 2018, "MATLAB Version 9.4 (R2018a)," The MathWorks, Natick, MA.

[51] Zajac, F. E., 1989, "Muscle and Tendon: Properties, Models, Scaling, and Application to Biomechanics and Motor Control," CRC Crit. Rev. Biomed. Eng, **19**(4), pp. 359–411.

[52] Lee, D. D., and Seung, H. S., 1999, "Learning the Parts of Objects by Non-Negative Matrix Factorization," Nature, **401**(6755), p. 788.

[53] Lee, D. D., and Seung, H. S., 2000, "Algorithms for Non-Negative Matrix Factorization," Adv. Neural Inf. Process. Syst., pp. 556–562.

[54] Tresch, M. C., Cheung, V. C. K., and d'Avella, A., 2006, "Matrix Factorization Algorithms for the Identification of Muscle Synergies: Evaluation on Simulated and Experimental Data Sets," J. Neurophysiol., **95**(4), pp. 2199–2212.

[55] Ting, L. H., and Macpherson, J. M., 2005, "A Limited Set of Muscle Synergies for Force Control During a Postural Task," J. Neurophysiol., **93**(1), pp. 609–613.

[56] Torres-Oviedo, G., Macpherson, J. M., and Ting, L. H., 2006, "Muscle Synergy Organization Is Robust Across a Variety of Postural Perturbations," J. Neurophysiol., **96**(3), pp. 1530–1546.

[57] Bühlmann, P., and Van De Geer, S., 2011, *Statistics for High-Dimensional Data: Methods, Theory and Applications*, Springer Science & Business Media, Berlin.

[58] Bekey, G. A., 1964, "Optimization of Multiparameter Systems by Hybrid Computer Techniques—Part I," Simulation, **2**(2), pp. 19–32.

[59] Clark, D. J., Ting, L. H., Zajac, F. E., Neptune, R. R., and Kautz, S. A., 2010, "Merging of Healthy Motor Modules Predicts Reduced Locomotor Performance and Muscle Coordination Complexity Post-Stroke," J. Neurophysiol., **103**(2), pp. 844–857.

[60] Burdet, E., Osu, R., Franklin, D. W., Milner, T. E., and Kawato, M., 2001, "The Central Nervous System Stabilizes Unstable Dynamics by Learning Optimal Impedance," Nature, **414**(6862), pp. 446–449.

[61] Takahashi, C. D., Scheidt, R. A., and Reinkensmeyer, D. J., 2001, "Impedance Control and Internal Model Formation When Reaching in a Randomly Varying Dynamical Environment," J. Neurophysiol., **86**(2), pp. 1047–1051.

[62] Bong, M. R., and Di Cesare, P. E., 2004, "Stiffness After Total Knee Arthroplasty," JAAOS-J. Am. Acad. Orthop. Surg., **12**(3), pp. 164–171.
[63] Tonietti, G., Schiavi, R., and Bicchi, A., 2005, "Design and Control of a Variable Stiffness Actuator for Safe and Fast Physical Human/Robot Interaction," IEEE International Conference on Robotics and Automation (ICRA), Barcelona, Spain, Apr. 18–22, pp. 526–531.
[64] Brown, S. H. M., and McGill, S. M., 2005, "Muscle Force-Stiffness Characteristics Influence Joint Stability: A Spine Example," Clin. Biomech., **20**(9), pp. 917–922.
[65] Franklin, D. W., So, U., Kawato, M., and Milner, T. E., 2004, "Impedance Control Balances Stability With Metabolically Costly Muscle Activation," J. Neurophysiol., **92**(5), pp. 3097–3105.
[66] Kearney, R. E., Stein, R. B., and Parameswaran, L., 1997, "Identification of Intrinsic and Reflex Contributions to Human Ankle Stiffness Dynamics," IEEE Trans. Biomed. Eng., **44**(6), pp. 493–504.
[67] Rack, P. M. H., and Westbury, D. R., 1974, "The Short Range Stiffness of Active Mammalian Muscle and Its Effect on Mechanical Properties," J. Physiol., **240**(2), pp. 331–350.
[68] Cui, L., Perreault, E. J., and Sandercock, T. G., 2007, "Motor Unit Composition Has Little Effect on the Short-Range Stiffness of Feline Medial Gastrocnemius Muscle," J. Appl. Physiol., **103**(3), pp. 796–802.
[69] Kitatani, R., Ohata, K., Sato, S., Watanabe, A., Hashiguchi, Y., Yamakami, N., Sakuma, K., and Yamada, S., 2016, "Ankle Muscle Coactivation and Its Relationship With Ankle Joint Kinematics and Kinetics During Gait in Hemiplegic Patients After Stroke," Somatosens. Mot. Res., **33**(2), pp. 79–85.
[70] Rinalduzzi, S., Trompetto, C., Marinelli, L., Alibardi, A., Missori, P., Fattapposta, F., Pierelli, F., and Currà, A., 2015, "Balance Dysfunction in Parkinson's Disease," Biomed Res. Int., **2015**, pp. 1–10.
[71] Rodriguez, K. L., Roemmich, R. T., Cam, B., Fregly, B. J., and Hass, C. J., 2013, "Persons With Parkinson's Disease Exhibit Decreased Neuromuscular Complexity During Gait," Clin. Neurophysiol., **124**(7), pp. 1390–1397.
[72] Weiss, P. L., Hunter, I. W., and Kearney, R. E., 1988, "Human Ankle Joint Stiffness Over the Full Range of Muscle Activation Levels," J. Biomech., **21**(7), pp. 539–544.